

Topological boundary modes in jammed matter

Daniel M. Sussman,^{1,*} Olaf Stenull,¹ and T. C. Lubensky¹

¹*Department of Physics and Astronomy, University of Pennsylvania,
209 South 33rd Street, Philadelphia, Pennsylvania 19104, USA*

Granular matter at the jamming transition is poised on the brink of mechanical stability, and hence it is possible that these random systems have topologically protected surface phonons. Studying two model systems for jammed matter, we find states that exhibit distinct mechanical topological classes, protected surface modes, and ubiquitous Weyl points. The detailed statistics of the boundary modes shed surprising light on the properties of the jamming critical point and help inform a common theoretical description of the detailed features of the transition.

I. INTRODUCTION

Topological properties of operators defined as functions of wavevectors in the Brillouin zone (BZ) control and protect aspects of the bulk electronic spectrum and the nature of interface states [1–3] in a wide range of systems, including polyacetylene [4, 5], quantum Hall materials [6, 7], topological insulators [8–13], and Weyl semimetals [14–18]. Recent work [19–22] has shown that topology plays a similar role in protecting phonon spectra and interface states in ball-and-spring Maxwell lattices [23]. Maxwell lattices, which include the square, kagome, and twisted kagome [24] lattices in two dimensions and the simple cubic and pyrochlore lattices in three dimensions, are characterized under periodic boundary conditions by a perfect balance between the number of constraints and degrees of freedom, i.e., $N_B = dN$ where N_B is the number of lattice bonds occupied by springs, N is the number of sites and d is the spatial dimension (or equivalently $n_B = dn$, where n_B is the number of springs and n the number of sites per unit cell).

The initial work on generalized kagome lattices with 3-site unit cells [19] and fully-gapped phonon spectra (i.e., with zero modes only at wavenumber = 0) has been extended to 4-site-unit-cell generalized square lattices [25, 26] in two dimensions and pyrochlore lattices [27] in three dimensions, which exhibit topologically protected zero-modes, respectively, at points or along lines in the interior of the Brillouin zone (BZ). We refer to the latter as Weyl points or lines because of their strong analogy with topologically protected electronic states in Weyl [16, 17] and line-node semi-metals [15], as well as certain photonic crystals [28]. In addition, both experiment and theory have demonstrated the existence of phonon edge states [29–38] protected by broken time-reversal and/or inversion symmetry much as is the case in topological insulators. These investigations in the growing field of topological mechanics hold out the promise of eventually controllably tuning phononic metamaterials by marshalling their topological features.

Here we apply topological ideas to large disordered-unit-cell Maxwell lattices relevant to the jamming transition. Topologically protected surface modes may be particularly interesting in these systems, since the boson peak in the density of vibrational states and diverging length scales near the critical point of jammed systems have been explained by how the introduction of free surfaces changes the phonon spectrum [39–41]. We study two model ensembles related to jammed two-dimensional matter: disordered jammed sphere packings (JSP) generated via a compression-based algorithm [42] and generic periodic approximations of the Penrose tiling (GPT) [43–45]. Figure 1 shows representative examples of relatively small unit cells from these ensembles. The large size of the unit cells we investigate precludes the sort of systematic study of the full phase space of unit-cell configurations and their associated topological properties that has been carried out for small unit cell lattices. Instead we pursue a stochastic approach in which we sample lattices composed of different randomly configured, but periodically repeated unit cells, and imagine taking the large-unit-cell-size limit. The configurations we study almost always have Weyl points in their spectra; that is, almost none has a fully gapped spectrum for all nonzero wavenumbers k in the BZ. The distribution of Weyl points in the unit cell and their number changes with random configuration, leading to different distributions of zero modes at free surfaces, and thus to different topological characterizations, even at the $k = 0$ point most relevant to jamming. In jammed systems, the n -site unit cell is in fact the entire system (i.e., $n = N$). However, by studying lattices in which these unit cells are periodically repeated [46], we are able to identify surface modes that do not appear in the bulk spectrum and that penetrate an arbitrary number of unit cells into the bulk. We find that the distribution of surface-mode decay lengths undermines part of the standard cutting argument [39, 40] used to predict the density of states and the divergent length scale l^* .

The remainder of the paper is organized as follows. In Section II, we briefly describe our protocol for generating members of the JSP and GPT ensembles. We also detail how the topological index and protected surfaces modes of these lattices can be theoretically and numerically computed. Section III applies these ideas to our model

* dsussman@sas.upenn.edu

¹ † DMS and OS contributed equally to this work

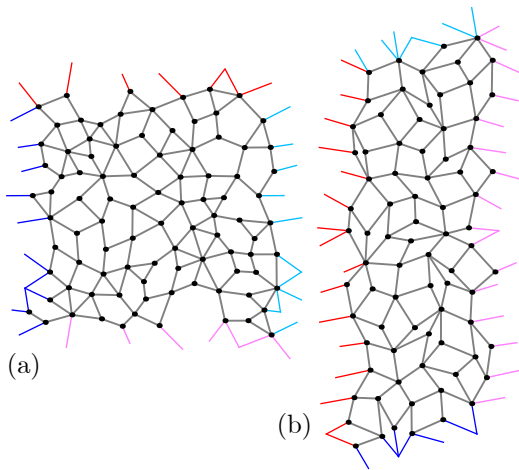


FIG. 1. Representative unit cells for (a) a jammed sphere packing (JSP) and (b) for generic Penrose tiling (GPT). These unit cells represent the entire sample under periodic boundary conditions in models of jamming. We periodically repeat them so as to create excitations with nonzero wavenumber k . The models of jammed solids correspond to the zero k limit of the periodic lattices. The edge bonds shown in dark red and blue are the ones that are cut to liberate the cell from periodic boundary conditions. The pink and light blue bonds are identical to the dark ones under periodic boundary conditions with a single unit cell.

disordered systems, and demonstrates that these large-unit-cell systems possess a correspondingly large number of topologically protected modes including Weyl modes and edge modes both at free surfaces and at domain walls which connect cells of differing topological character. In Section IV, we present detailed statistics of the edge modes in our systems, and discuss the implications of those statistics for the “cutting argument” [39, 40] commonly used to explain properties of jammed systems. We close in Section V with a brief summary.

II. MODELS AND METHODS

A. Construction of lattices

We produce our model networks as follows: For the JSP, we numerically generate packings of N particles in two dimensions by starting with a dense (i.e., above the jamming transition) polydisperse mixture of discs with a flat distribution of particle sizes between σ and 1.4σ , where σ is the unit of length. The interaction between particles is modeled by a harmonic soft repulsive potential [42]. The discs are initially placed at random (i.e. in an infinite-temperature configuration) in a square simulation box with periodic boundary conditions. The system is then rapidly quenched to zero temperature by combining line-search methods, Newton’s method, and the FIRE algorithm [47]. The average coordination number is changed by incrementally expanding or compress-

ing the system uniformly and then re-quenching to zero temperature; this is repeated until $n_B = dn$, that is, until we obtain a Maxwell lattice. The soft disc packing is converted to the “unstressed” network [48, 49], replacing each pairwise interaction with an un-stretched harmonic spring between nodes at the particle centers.

For the GPT, we use the standard projection procedure from the five-dimensional hypercube \mathbb{Z}^5 onto a two-dimensional space [50]. The orientation of the plane in hyperspace that leads to the quasiperiodic rhombus tiling [51] is related to the golden ratio τ . Approximating τ by the ratios τ_m of successive Fibonacci numbers ($\tau_1 = 1/1$, $\tau_2 = 2/1$, $\tau_3 = 3/2$, ...) gives the periodic approximants. These are rhombic tiles arranged in rectangular unit cells of increasing size that approach the quasiperiodic tiling as $m \rightarrow \infty$. We randomly displace nodes by a small amount without changing the connectivity of the approximants, and then replace the edges of the (deformed) tiles with un-stretched harmonic springs.

B. Edge states and topological characterization

The vibrational properties of elastic networks consisting of periodically repeated unit cells with n sites and n_B bonds can be described [52] by the $n_B \times dn$ compatibility matrix $C(k)$, relating bond displacements $u(k)$ to bond extensions $e(k)$ via $C(k)u(k) = e(k)$, and the $dn \times n_B$ equilibrium matrix $Q = C^\dagger(k)$, relating bond tensions $t(k)$ to site forces $f(k)$, for each wavenumber k in the BZ. The null space of $C(k)$ consists of zero modes whose displacements do not stretch bonds; that of $Q(k)$ consists of states of self stress (SSS) in which bonds under tension exert no net forces at sites. When masses and spring constants are all set to unity, the dynamical matrix determining the phonon spectrum is simply $D(k) = Q(k)C(k)$. In periodic systems, the Calladine-Maxwell theorem [20, 52] generalizes to $n_0(k) - s(k) = dn - n_B$ for every k , where $n_0(k)$ is the number of zero modes and $s(k)$ the number of SSS. In periodic Maxwell lattices where $dn = n_B$ there is always one SSS for each zero mode.

The term “isostatic” rather than “Maxwell” is commonly used to identify lattices with $N_B = dN$. This term, however, strictly speaking only applies to finite lattices (frames) [53, 54] with no SSSs and only zero modes corresponding to the $d(d+1)/2$ rigid translations and rotations d -dimensions, i.e. to “statically determinate” lattices. Under periodic boundary conditions, things are complicated in $N_B = dN$ lattices by the presence of zero energy elastic distortions of the unit cell, called Guest modes [20, 55, 56], but it is reasonable to use the term “isostatic” for Maxwell lattices ($n_B = dn$) with exactly d zero modes and d SSSs. Thus periodic isostatic lattices are a subset of periodic Maxwell lattices, and Maxwell lattices with Weyl modes are not isostatic.

1. Winding numbers and domain walls

The determinant of $C(k)$ (or $Q(k)$) provides a map from the BZ to the complex plane. Any path in wavenumber space starting and ending at points separated by a reciprocal lattice vector G is mapped to a closed loop in the complex plane characterized by a winding number. For simplicity, we consider straight paths parallel to reciprocal lattice vectors indexing sets of lattice planes perpendicular to them. Let p be the component of k parallel to G and q the component parallel to these planes. Then $\det C(q, G) \equiv \det C(q, p, G)$ depends on p through $z = e^{i2\pi p/G}$, where $G = |G|$. The winding numbers,

$$n(q, G) = \frac{1}{2\pi i} \int_0^G dp \frac{d}{dp} \ln \det C(q, p, G), \quad (1)$$

depend in general on q along a surface as well as G . In the small-unit-cell systems previously considered this integral either vanished or gave ± 1 , but in general it can take any integer value bounded by the number of bonds cut by the surface. The matrices $C(k)$ and $\det C(k)$ also depend on the choice of unit cell as depicted in Fig. 2 (a). If the cell is chosen so that it is “surface compatible”, i.e., so that it has no nodes or “dangling” bonds outside a lattice bounded by a surface coinciding with a lattice plane indexed by G , then the local contribution to the surface zero mode count vanishes and the winding number computed by Eq. (1) gives the number of zero modes localized on that surface: $n_0^S(q, G) = n(q, G) \geq 0$. If a portion of the lattice under periodic boundary conditions is liberated by cutting two parallel free surfaces that remove Δn_B bonds (for simplicity, we do not consider removal of sites as well), then the total number of zero modes on the two surfaces is $n_{0,\text{tot}} = n_0^S(q, G) + n_0^S(q, -G) = \Delta n_B$.

At a domain wall separating “left” and “right” lattices, the $q \neq 0$ topological count [20] of the difference between the number of domain-wall zero modes, $n_0^D(q, G)$, and SSS, $s^D(q, G)$, is $\nu^D(q, G) \equiv n_0^D(q, G) - s^D(q, G) = n_{0,-}^S(q, G) + n_{0,+}^S(q, -G) - \Delta n_B$, where $n_{0,\mp}^S(q, \pm G)$ are the number of zero modes of the left and right free surfaces that will constitute the domain wall and Δn_B is the number of bonds per unit cell needed to bind the two free surfaces together. Domain walls prepared in this way can have either zero modes ($\nu^D(q, G) = n_0^D(q, G)$) or SSS ($\nu^D(q, G) = -s^D(q, G)$). The topological properties of fully-gapped Maxwell $2d$ -lattices, like the kagome and some realizations of the 4-site-unit-cell square lattice, are fully determined by a polarization vector $R_T = -\sum n(q, b_i) a_i$, where a_i and b_i are the basis vectors of the direct and reciprocal lattice, respectively, and $n(q, b_i)$ is independent of q . A useful but q -dependent measure of topological character in systems with Weyl points is $\nu^W(q, G) = [n_0^S(q, G) - n_0^S(q, -G)]/2$, which reduces to $R_T \cdot G/(2\pi)$ in gapless systems in agreement with reference [19].

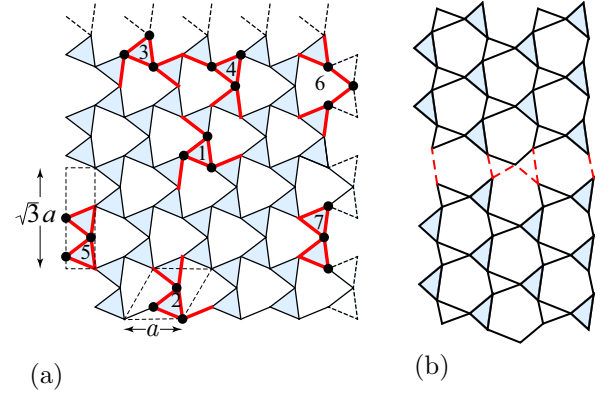


FIG. 2. (a) A section of a twisted kagome lattice showing dashed bonds at the top and right edges that are cut to liberate the multi-unit cell lattice from periodic boundary conditions on a torus. Also shown are different unit cells, including a symmetric unit cell (1) that is not compatible with the surfaces and various surface compatible unit cells (2-7). (b) An example of a domain wall, whose bonds are dashed, connecting two lattices with different topological polarization.

Since the $q = 0$ limit is of particular interest in jammed systems, we note that when $q = 0$ the topological count at a domain wall is slightly modified by the presence of the global translational zero modes. The counting of the number of zero modes at a free surface includes these global translational modes, relative rigid translations of the cells on either side of the domain wall, and the $\tilde{n}_{0,\pm}^S(0, G)$ of exponentially decaying surface modes. Thus, there are a total of $\tilde{n}_{0,\pm}^S(0, G) + d$ zero modes at the \pm surfaces. As when $q \neq 0$, the creation of the domain wall requires Δn_B extra constraints, and the total number of domain-wall zero modes (excluding global translations is)

$$\begin{aligned} \tilde{\nu}^D(0, G) &= \tilde{n}_{0,+}^S(0, G) + d + \tilde{n}_{0,-}^S(0, G) + d - \Delta n_B - d \\ &= \tilde{n}_{0,+}^S(0, G) + \tilde{n}_{0,-}^S(0, G) + d - \Delta n_B. \end{aligned} \quad (2)$$

This count includes d modes in which the $+$ and $-$ surfaces translate rigidly with respect to each other. These modes can in general mix with the exponentially decaying modes.

2. Structure of surface modes

The winding numbers computed via Eq. (1) provide a count of the number of zero modes at a free surface. Much more information about these modes can be extracted from the compatibility matrix. The lattice can be divided into contiguous layers, one unit cell thick and composed of parallel contiguous surface-compatible unit cells starting at the free surface and penetrating inward. This construction allows the compatibility matrix to be Fourier transformed parallel to the layers to produce a banded matrix $C(q, G)$ [20]. The main diagonal

of this banded matrix is composed of $dn \times n_B$ submatrices $C_{11}(q, G)$; the C_{11} are compatibility matrices that describe the relationship of node motions to bond extensions for nodes and bonds entirely within a layer. These are indicated, e.g., by the gray and blue bonds in Fig. 1. The diagonal in C above the main diagonal is composed of identically-sized submatrices $C_{12}(q, G)$, which connect bonds in one layer to sites in the next layer, indicated by the red bonds in Fig. 1. For a fully periodic system with no surface, by construction $C(q) = C_{11}(q) + C_{12}(q)$.

In this construction, a set of displacements $\mathbf{U} = (\mathbf{u}_1, \mathbf{u}_2, \dots)$, where \mathbf{u}_i is a set of displacements in unit cell i , will be a zero mode if $C_{11}\mathbf{u}_i + C_{12}\mathbf{u}_{i+1} = 0$. These equations, in turn, are solved by $\mathbf{u}_{i+1} = \lambda\mathbf{u}_i$ if

$$\det(C_{11} + \lambda C_{12}) = 0, \quad (3)$$

and modes decay as $\lambda = \exp(-\kappa r)$ with distance r (in units of the unit-cell size) away from the free surface when $\lambda < 1$. In general, the inverse penetration depth κ is complex, indicating a surface mode that decays exponentially with oscillations. The sign of $\tilde{\kappa} = \text{Re}(\kappa)$ determines which surface the zero mode is localized to: positive (negative) $\tilde{\kappa}$ goes with the surface bounding an interior toward positive (negative) r .

For small- n unit cells this prescription works well. In general, though, evaluating the determinant of a large, sparse matrix and finding the roots of the resulting polynomial in λ is both slow and numerically unstable, making it difficult to find all of the localized surface modes. However, if C_{11} is an invertible matrix (implying no zero mode localized completely in the surface unit cell), the problem can be reduced to finding the eigenvalues S_j of $S \equiv C_{11}^{-1}C_{12}$: the λ 's that satisfy Eq. (3) are determined by the set of non-zero S_j , $\lambda_j = -S_j^{-1}$. For the GPT up to the 8/5 approximant ($n = 1440$), we were always able to choose a unit cell with an invertible C_{11} . For jammed unit cells it becomes increasingly hard with increasing n to find unit cells with an invertible C_{11} , implying the existence of zero modes completely localized within the unit cell adjacent to the free surface. This is not surprising in light of existing data on the prevalence of surface “rattlers” in the presence of cut surfaces [57]. Nevertheless, in Section IV we will show that these surface rattlers do not seem to affect the distribution of the other surface modes of the system.

III. TOPOLOGICAL MODES OF DISORDERED SYSTEMS

A. Surface and Weyl modes

Figure 3 illustrates a topological characterization for a typical realization of the 1/1 approximant of the GPT. The plot shows the number n_+ (n_-) of surface zero modes with positive (negative) $\tilde{\kappa}$ as a function of wavevector. The discontinuous jumps in the topological class as a

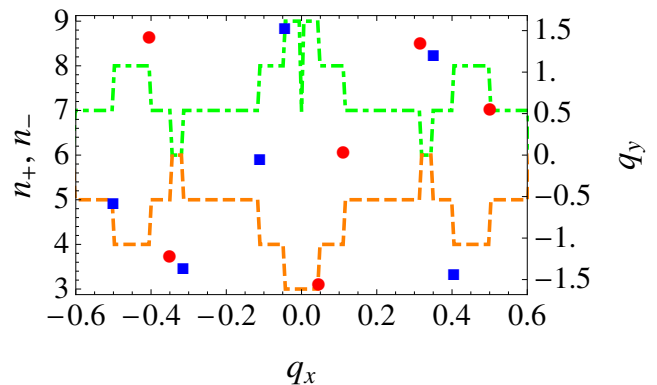


FIG. 3. (Color online) Number n_+ of surface zero modes with positive $\tilde{\kappa}$ (green dot-dashed line) and number n_- with negative $\tilde{\kappa}$ (orange dashed line) for a typical 1/1 approximant (which has 30 sites per unit cell) as a function of q_x . Square (blue) and circular (red) points indicate the location (with q_y on the right ordinate) of Weyl points with positive and negative charge, respectively. The uniform translation modes at $q = 0$ are not included, and hence $n_+ + n_-$ decreases by $d = 2$ at $q = 0$. The topological count is $\tilde{\nu}^W(0, G) = (7-3)/2 = 2$.

function of $q = q_x$ imply the presence of Weyl-type singularities. To locate these singularities, we calculate the winding numbers (given by Eq. (1), but for small closed square loops instead of straight integration lines) around points in the BZ. These integrals yield 0, -1 or $+1$, indicating the absence or, respectively, presence of a Weyl point with charge -1 or $+1$. Here, there are $N_{\text{Weyl}} = 12$ Weyl points that come in pairs of opposite charge at positions \mathbf{k} and $-\mathbf{k}$. Discontinuous changes in n_+ and $n_- = \Delta n_B - n_+$ occur at projections of these points onto the q_x axis and have a magnitude equal to the winding number of the of the Weyl point. We note that for this example $n_+(q = 0) \neq n_-(q = 0)$. This indicates that, in the $q = 0$ limit of particular relevance for jammed systems, we can find states with non-trivial topological character.

In general we find that our disordered systems have an increasing number of Weyl points as the size of the unit cell grows. This data is shown in Fig. 4 for the JSP ensemble and unit cell sizes between $n = 16$ and $n = 96$. Both the mean and the distribution of the number of Weyl points in a given realization of the disordered system scales approximately as $n^{2/5}$, although given the discrete nature of the distribution exponents in the range $1/3$ to $1/2$ collapse the data in the figure almost as well. For states in the GPT ensemble the scaling is similar. Reference 46 carefully studied the negative eigenvalues that sometimes appear at finite wavevectors in hyperstatic sphere packings under pressure, and attributed these instabilities to stress. In our systems, applying a small pressure term while fixing the contact network would generically push the Weyl modes we have found to negative frequencies. Thus, the question of whether the Weyl points in this work and the stress-induced in-

stabilities of Ref.46 are independent and complementary instabilities or if they are linked to each other away from the Maxwell lattice limit is an interesting open question. Also interesting is whether any of the Weyl modes we have found here survive in mildly hyperstatic but unstressed packings.

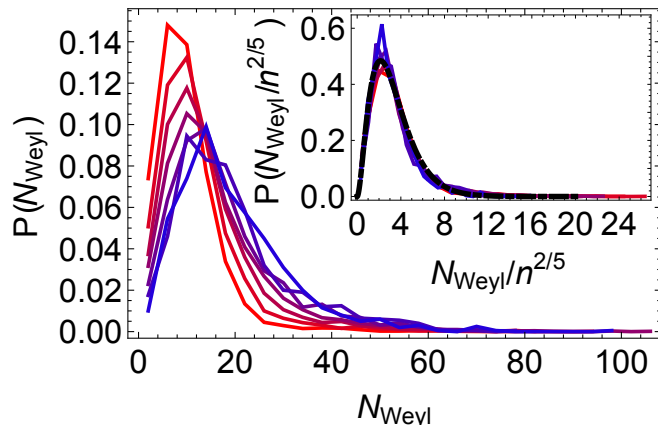


FIG. 4. (Color online) Probability distribution of the number of Weyl points for JSP with $n = 16, 24, 32, 48, 64, 80, 96$ (red, narrowly peaked to blue, broad curves). The inset shows the curves in the main frame scaled by $n^{2/5}$, together with a fit to a gamma distribution with parameters $k = 2.83$ and $\theta = 0.582$ (black, dashed curve).

B. Domain-wall modes

To study topologically protected phonons localized at domain walls separating different topological classes, we construct Maxwell “supercells” by joining two lattices with unit cells A and B – which have the same number of boundary bonds – in the sequence $A \cdots AB \cdots BA \cdots A$. Unit cells at the AB and BA interfaces are linked with the appropriate number of bonds to preserve the Maxwell relation $dn = n_B$ when periodic boundary conditions are applied to the outer A ’s, but otherwise the linking bonds are arbitrary. In Fig. 5 we show a representative example for a JSP lattice with a total of $10A$ and $10B$ cells, each with $n = 64$ sites, and focus on calculating the normal modes of the system at $q = 0$. We chose the A and B lattices to be in different topological classes, according to the value of the winding number calculated with Eq. (1). In an infinite system, one would, therefore, expect that one of the domain walls would exhibit zero modes and the other SSS. In our finite system, interaction between these two domain walls raise the frequency of zero modes to (exponentially small) nonzero values. And indeed, a direct numerical evaluation of the eigenmodes of the dynamical matrix (and the dual matrix $\mathcal{M}(\mathbf{k}) = \mathbf{C}(\mathbf{k} = 0)\mathbf{Q}(\mathbf{k} = 0)$) reveal that there is a zero mode (in the infinite size limit) at one of the two interfaces, and as demanded by the Calladine-Maxwell

count [52], a balancing SSS which is located at the other.

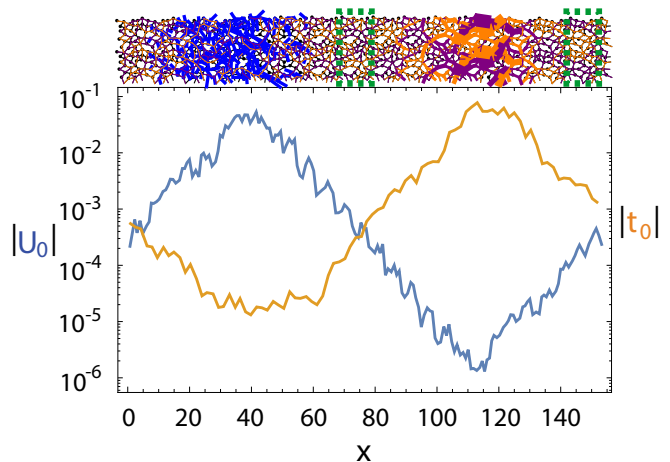


FIG. 5. (top) State of self stress and zero mode localized at the interface between jammed unit cells with $n = 64$ of different topological classes. The large, rectangular unit cell is under periodic boundary conditions in both directions. Dashed boxes highlight the unit cells that are repeated and glued together to form the supercell. (bottom) Total magnitude of the topologically protected zero mode (blue) and state of self stress (yellow) in vertical slices of the combined unit cell. The exponentially localized character of each, with oscillations, is clearly seen.

As discussed above, there can be more than one zero mode per wavenumber q along a domain wall, since it is the combination $n_{0-}^S(0, \mathbf{G}) + n_{0+}^S(0, -\mathbf{G}) - \Delta n_B$ that determines the number of interfacial zero modes or SSS at a domain wall. By carefully selecting different unit cells on either side of a domain wall it should be possible to create an interface that hosts multiple topologically protected modes localized to the domain wall. We present such an example here. As noted above, the exponentially decaying surface modes will have a small, non-zero frequency when they are inserted into the finite $A \cdots AB \cdots BA \cdots A$ supercells we use (related to the magnitude of the exponentially decaying mode when it encounters the next interface). One way of detecting them, then, is to look for modes whose frequencies become exponentially small as more and more copies of A and B are used in the construction of the supercell. This is shown in Fig. 6. While many of the modes decay as a power law with increasing system size and are thus easily identified as being low-frequency disordered plane waves, we see two modes whose energy scale drops exponentially fast. This is a clear signature of modes exponentially localized to an interface in the supercell. As illustrated in Fig. 7, which shows the bonds participating in the two distinct SSSs, these multiple interfacial modes can readily be visualized. There are of course compensating domain walls with zero modes, not shown in the figure.

IV. STATISTICS OF SURFACE MODES

A. Distribution of penetration depths

Now, we turn to the statistics of surface zero modes at $q = 0$ for surfaces parallel to the x -axis. In GPTs this corresponds to the x direction of the undistorted Penrose tiling and in JSP to one of the faces of the simulation cell (the JSP have no unit-cell anisotropy, so the

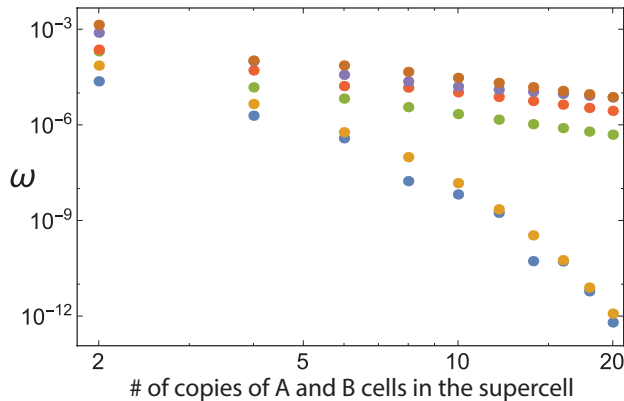


FIG. 6. Frequencies (square-root of the energetic cost) of the lowest vibrational modes at the interface of jammed unit cells of different topological classes as a function of how many times the unit cells were copied. Here we see two modes with exponentially decaying frequency, together with four disordered plane waves modes with a power-law decay.

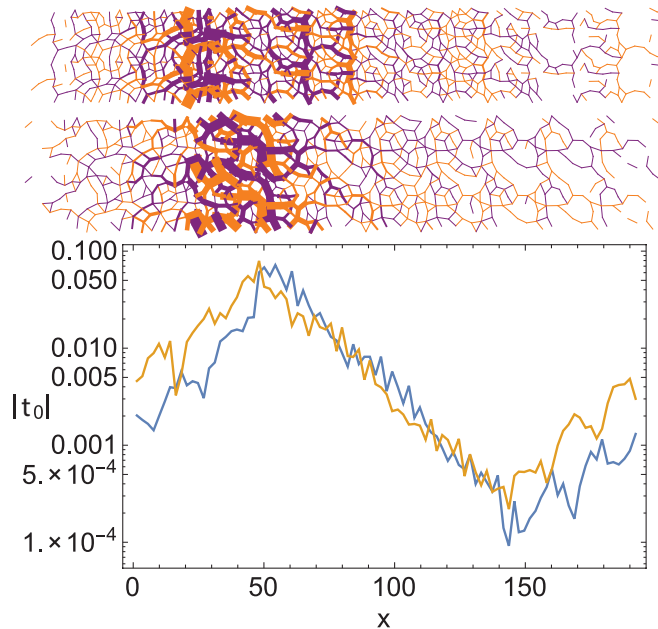


FIG. 7. (top) Two independent states of self stress localized at the interface between tiled jammed unit cells of $n = 24$ with $\nu^d(0, y) = 2$. For clarity, bonds whose stress is below a threshold are not shown.

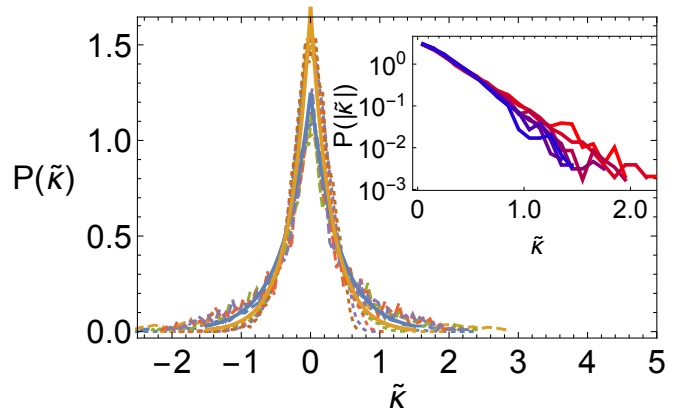


FIG. 8. (Color online) Probability distribution of $\tilde{\kappa}$ for (dotted lines) JSP with $n = 16, 24, 32, 48, 64, 80, 96, 128$ and (dashed lines) GPT approximants $1/1, 2/1, 3/2, 5/3, 8/5$, corresponding to $n = 30, 80, 210, 550, 1440$. Solid lines are best exponential fits to $P(\tilde{\kappa}) \approx \exp(-|\alpha\tilde{\kappa}|)\alpha/2$ for $\alpha = 2.5$ and $\alpha = 3.4$ for the GPT and JSP, respectively, for all data points independent of lattice size. (inset) Log plot of $P(|\tilde{\kappa}|)$ for JSP with $n = 16$ (top, red curve) to $n = 96$ (bottom, blue curve). Note the small but noticeable increase in decay rate with increasing system size.

distinction between x and y is unimportant). We place no restriction on depth perpendicular to the x -axis, so we can access penetration lengths that span an arbitrary number of unit cells into the bulk, and we average over many random realizations of our model systems (e.g., 1000 for the $1/1$ GPT). The distributions $P(n_+)$ and $P(n_-)$ of n_+ and n_- for both JSP and GPT are approximately Gaussian with mean given by half the number of bonds that are cut to produce the free surface ($\sim \sqrt{n}$) and a variance that grows as $\sim n^{1/4}$. Figure 8 shows the probability distributions of the inverse penetration depths, $P(\tilde{\kappa})$, omitting the delta-function spike at $\tilde{\kappa} = 0$ associated with the trivial translations. Both associated $P(\tilde{\kappa})$ s can be approximated by exponential distributions, albeit with different variances. The distributions for the JSP and GPT are characterized by a slightly different expected penetration depth, and the main plot suggests that the typical decay lengths do not grow strongly with system size. However, zooming into the tails of the distribution suggests that a very modest system-size effect may be present, a point we discuss later.

B. Effect of surface rattlers on JSP statistics

In the previous sections, we studied lattices with square unit cells with invertible C_{11} matrices that necessarily had no surface zero modes with nonzero amplitude restricted to the first layer of the lattice because if they did, there would have to be a displacement vector u such that $C_{11}u = 0$ contradicting the assumption that C_{11} is invertible. However, systems at the jamming threshold typically have surface rattlers when free surfaces are in-

troduced, and the probability of finding a configuration with an invertible C_{11} decays rapidly as the system size increases. In Fig. 9, we take a representative subset of JSP with system size N generated by the compression algorithm, which we denote JSP_N , and plot the fraction of these states with an invertible C_{11} . For those states with a non-invertible C_{11} , some modes exist that are necessarily localized entirely within the surface unit cell but they may, nevertheless, involve particles far from the free surface. Note, though, that the machinery developed in Section II can still be used (albeit by directly solving $\det(C_{11} + \lambda C_{12}) = 0$ rather than using the eigenvalue techniques) to investigate penetration depth statistics, and noting that when C_{11} is not invertible one must be careful to include not only the topological count discussed in this work but also a local zero-mode count of the surface cell relative to that of the bulk cell (this is captured by the “dipole moment” R_L , which allows one to express the local zero-mode count via $R_L \cdot G/(2\pi)$, as discussed in Refs.[19, 20])

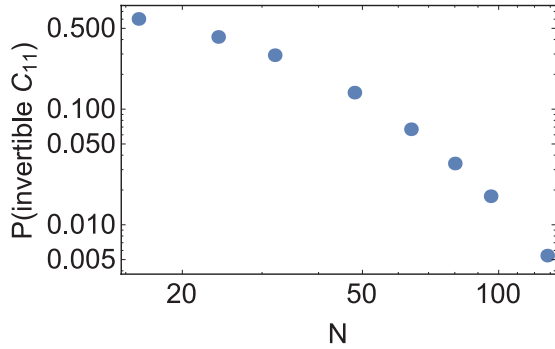


FIG. 9. Probability that a random compression-algorithm-generated jammed configuration with N sites will have a choice of square unit cell for which C_{11} is invertible.

To check whether our results are sensitive to sampling over only those jammed unit cells that have an invertible C_{11} , we compare the distribution of inverse penetration depths, $P(\tilde{\kappa})$, for both JSP_N and $\{JSP_N | \exists C_{11}^{-1}\}$. To do this we chose an n small enough that $\det(C_{11} + \lambda C_{12}) = 0$ can be reliably solved numerically to collect penetration depth statistics for any member of $\{JSP_N\}$. Figure 10 shows the result of this for $n = 32$, leading us to expect that the results presented elsewhere in this paper are not biased by averaging over the sub-ensemble of JSP for which C_{11} is invertible.

C. The overlap function

Our explicit decomposition of the nullspace of C into its constitutive surface modes provides insight into the physics of the jamming transition. One common understanding of the origin of the plateau in the density of states near the transition proceeds via a variational argument on the behavior of the eigenvectors of the dynamical

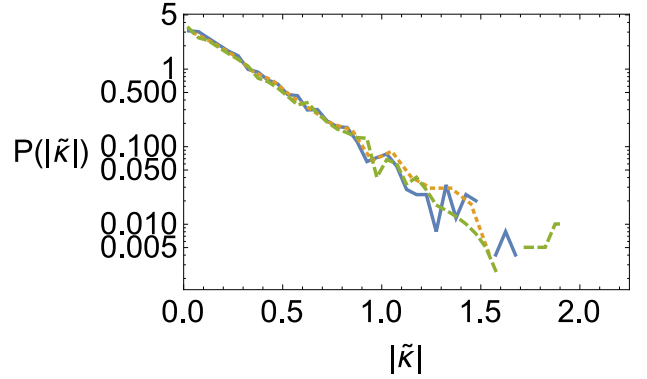


FIG. 10. Probability distribution of penetration depths for different sampling and numerical methods for $n = 32$ JSP. The blue solid and yellow dotted lines use the eigenvalue and determinant methods, respectively, of determining $\tilde{\kappa}$ for JSP for which C_{11} is invertible. The dashed green line uses the determinant method and averages over JSP regardless of whether C_{11} is singular.

matrix D when periodic boundary conditions are replaced by free boundaries [57]. This standard argument relies on an assumption about the total structure of the nullspace of the free-surface system. Assuming that boundaries normal to x at $x = 0$ and $x = L_x$ are replaced by free surfaces, this assumption is conveniently written in terms of the overlap function [40]:

$$f(x)dx = n_{0,\text{tot}}^{-1} \sum_{\beta=1}^{n_{0,\text{tot}}} \sum_{x_i \in [x, x+dx]} |u_{i,\beta}|^2. \quad (4)$$

where $0 \leq x < L_x$, β labels the $n_{0,\text{tot}} = \Delta n_B$ zero modes, $u_{i,\beta}$ denotes the displacement of site i in mode β , and x_i is the x coordinate of the reference position of site i . The original variational argument for configurations at the jamming threshold assumed that $H_1 = \min[L_x f(x)]$ is bounded from below by a constant that is independent of linear system size [40, 57].

The overlap function, averaged over many realizations of the disorder, is directly related to $P(\tilde{\kappa})$. Assuming that the inverse penetration depth of each exponentially localized zero mode is independently drawn from the $P(\tilde{\kappa})$, a straightforward calculation detailed later in this section connects $P(\tilde{\kappa})$ to $f(x)$. Intuitively, the fact that we do not observe strong shifts in $P(\tilde{\kappa})$ towards more slowly decaying modes with increasing system size suggests that $H_1(n)$ is a monotonically decreasing function, and our analytical arguments presented below confirm that $H_1(n)$ is not bounded from below by a positive constant. As we show in Fig. 11, this expectation is also numerically confirmed by further simulations of JSP Maxwell lattices from which free surfaces are cut. This undermines part of the variational argument [39, 40] for the jamming transition, which directly connects the lower bound on H_1 to an upper bound on the energetic cost of potential low-frequency vibrations. We note that this finding is not re-

stricted to two-dimensional JSP lattices; directly studying the overlap function for three-dimensional jammed Maxwell lattices also shows that $H_1(n)$ is a monotonically decreasing function of system size.

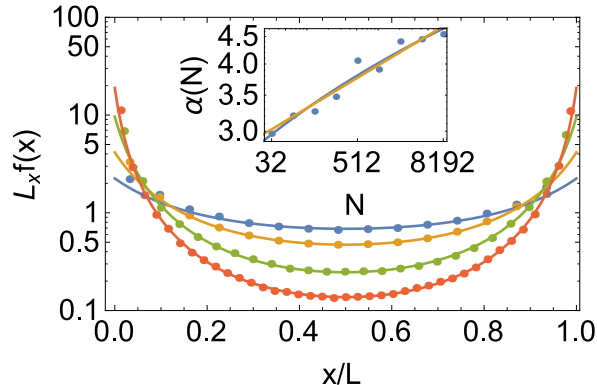


FIG. 11. Numerically obtained overlap function defined in Eq. (3) of the main text for jammed two-dimensional unit cells with $n = 64, 256, 1024, 8192$ (points, top to bottom), together with the fit based on Eq. (9) (lines). Inset: Best-fit value of α as a function of system size, together with logarithmic and power-law fits to the data. Here the power-law exponent is < 0.1 .

Without this upper bound, our understanding of the jamming boson peak is once again uncertain, although we note that effective-medium calculations (e.g. Ref. 58) and a very recent variational argument[59] also treat the behavior of the density of states near the jamming transition. Rather than performing a variational calculation on the effect of introducing free surfaces, the most recent variational work considers the dipolar response generated by elongating bonds added to an isostatic network. The argument, which is supported by numerical results, assumes that the characteristic volume of the dipolar response field scales as $1/\Delta Z$, where ΔZ is the distance of the lattice from the jamming transition, and that the magnitude of the response is of similar magnitude everywhere in this volume and does not decay strongly with distance. That the response field has a volume that scales as $1/\Delta Z$ is supported both by direct studies of the response to bond elongation[60] and also recent work looking at the SSS associated with the existence of a given bond in a hyperstatic packing[61]. The evidence that the magnitude of the dipolar response is roughly constant in this volume may need further study, as there is evidence that typical states of self stress have a (stretched-) exponentially decaying spatial profile in the volume of interest. The relationship between this observation and averages over typical dipolar response fields generated by bond elongation is a subject of current investigation.

We now show how the overlap function can be related to the distribution of penetration depths obtained earlier. While this may be surprising, given that the topological characterization above dealt with the surface modes of semi-infinite systems and not with the fully liberated sys-

tems considered by the cutting argument, we note that the exponentially decaying zero modes of a semi-infinite system are also valid zero modes for a system truncated by a second free surface. Thus, we fully expect the behavior of the overlap function for a single unit cell liberated by parallel free surfaces to be determined by the statistics of the surface modes deduced in the semi-infinite case considered above.

Restricting ourselves to the two-dimensional case, we approximate the number of zero modes in the cut system by the surface area of the cut, (since this is proportional to the number of bonds cut), $n_0 \sim L$, and note that the number of sites in the interval $x_i \in [x, x + dx]$ is $\rho L dx$ where ρ is the number density of sites in the unit cell. Finally, we note that the modes $|u_{i,\beta}|^2$ are normalized:

$$\int_0^L |u(x)|^2 \rho L dx = 1. \quad (5)$$

If the average magnitude of mode β at x ,

$$u_\beta(x) = (\rho L dx)^{-1} \sum_{x_i \in [x, x+dx]} u_{i,\beta}, \quad (6)$$

is independent of x (as is the case for the translational modes) then this normalization sets

$$|u_{\text{trans}}(x)|^2 = 1/\rho L^2. \quad (7)$$

On the other hand, if $u_\beta(x)$ has an exponentially decaying profile with inverse penetration depth $\tilde{\kappa}$ then the normalization condition sets

$$|u_{\text{exp}}(x)|^2 = \frac{2\tilde{\kappa} |\exp(-x\tilde{\kappa})|^2}{\rho L (1 - \exp(-2L\tilde{\kappa}))}. \quad (8)$$

Of the L zero modes there will be two translational zero modes, and $(L - 2)$ exponentially decaying modes with inverse penetration depth drawn from the distribution $P(\tilde{\kappa})$. Averaging over many realizations of the cut Maxwell-lattice jammed configurations, we have

$$\langle f(x) \rangle \approx \frac{2}{L} |u_{\text{trans}}(x)|^2 \rho L + \frac{L-2}{L} \langle |u_{\text{exp}}(x)|^2 \rangle \rho L, \quad (9)$$

where

$$\langle |u_{\text{exp}}(x)|^2 \rangle = \int_{-\infty}^{\infty} P(\tilde{\kappa}) \frac{2\tilde{\kappa} |\exp(-x\tilde{\kappa})|^2}{\rho L (1 - \exp(-2L\tilde{\kappa}))} d\tilde{\kappa}. \quad (10)$$

Taking the distribution of $\tilde{\kappa}$ to be exponential, $P(\tilde{\kappa}) \approx (\alpha/2) \exp(-|\alpha\tilde{\kappa}|)$, the above integral can be written in terms of the first derivative of the digamma function, $\psi'(z)$:

$$\langle |u_{\text{exp}}(x)|^2 \rangle = \frac{\psi'(\frac{1+2\alpha x}{2\alpha L}) + \psi'(\frac{1-2\alpha x}{2\alpha L})}{4\alpha \rho L^3} \quad (11)$$

Substituting Eqs. (7, 11) in Eq. (9) then gives an expression for the overlap function averaged over many realizations of the disorder. We plot this in Fig. 11 for

different values of n . The inset to Fig. 8 shows that the decay rate of $P(\tilde{\kappa})$, i.e., the value of α , increases with increasing n . Adjusting α to provide the best fit to the overlaps functions for different n yields the solid curves in Fig. 11. The exponent α increases from approximately 3 to 4.5 as n increases over two orders of magnitude from 32 to 8192. This suggests that, for the two-dimensional JSP, the mean of $P(\tilde{\kappa})$ may be logarithmically increasing with system size. Understanding precisely what controls the observed α for these disordered systems is an open challenge.

V. SUMMARY

In summary, we have studied topologically protected boundary modes and k -localized Weyl modes in large-unit-cell lattices derived from model jammed systems. In addition to computing winding numbers to identify the topological classes of our lattices, we have extended the formalism in Ref. [20] to compute complete sets of exponential decay profiles for all elements in the nullspace of C for large systems with free surfaces. We discovered

that randomized Penrose tilings and jammed unit cells are a rich source of lattices that can take on a topologically non-trivial character. Furthermore, the structure of these topologically modes indicate an interesting inconsistency in an argument explaining one of the most prominent features of the jamming transition, pointing towards the need for a more complete theory. Finally, the close correspondence between the GPT and JSP, previously documented for their elastic properties [43] and here observed in their topological characterization, further corroborates the idea that generic Penrose tilings are useful model systems for jammed matter.

ACKNOWLEDGMENTS

We thank Bryan Chen for making the RigidityPackage available [62], with which Figs. 5, 7 were made. This work was supported by NSF under grants DMR-1104707 and DMR-1120901 (TCL and OS) and by the Advanced Materials Fellowship of the American Philosophical Society (DMS). TCL is grateful for support from a Simons Fellows grant.

-
- [1] N. Nakamura, *Geometry, Topology and Physics*, 2nd ed. (Institute of Physics Publishing, Bristol, 2008) p. 79 and chapter 12.
 - [2] G. E. Volovik, *The Universe in a Helium Droplet* (Clarendon, Oxford, 2003).
 - [3] G. Volovik, *Lecture Notes in Physics* **718**, 3173 (2007).
 - [4] W. P. Su, J. R. Schrieffer, and A. J. Heeger, *Phys. Rev. Lett.* **42**, 1698 (1979).
 - [5] R. Jackiw and C. Rebbi, *Phys. Rev. D* **13**, 3398 (1976).
 - [6] B. I. Halperin, *Phys. Rev. B* **25**, 2185 (1982).
 - [7] F. D. M. Haldane, *Phys. Rev. Lett.* **61**, 2015 (1988).
 - [8] C. L. Kane and E. J. Mele, *Phys. Rev. Lett.* **95**, 146802 (2005).
 - [9] B. A. Bernevig, T. L. Hughes, and S.-C. Zhang, *Science* **314**, 1757 (2006).
 - [10] J. E. Moore and L. Balents, *Phys. Rev. B* **75**, 121306 (2007).
 - [11] L. Fu, C. L. Kane, and E. J. Mele, *Phys. Rev. Lett.* **98**, 106803 (2007).
 - [12] Z. Hasan and C. Kane, *Rev. Mod. Phys.* **82**, 3045 (2010).
 - [13] X.-L. Qi and S.-C. Zhang, *Rev. Mod. Phys.* **83**, 1057 (2011).
 - [14] X. G. Wan, A. M. Turner, A. Vishwanath, and S. Y. Savrasov, *Phys. Rev. B* **83**, 205101 (2011).
 - [15] A. A. Burkov and L. Balents, *Phys. Rev. Lett.* **107**, 127205 (2011).
 - [16] A. A. Burkov, M. D. Hook, and L. Balents, *Phys. Rev. B* **84**, 235126 (2011).
 - [17] J. P. Liu and D. Vanderbilt, *Phys. Rev. B* **90**, 155316 (2014).
 - [18] S.-Y. Xu, I. Belopolski, A. Nasser, M. Neupane, G. Bian, C. Zhang, R. Sankar, G. Chang, Z. Yuan, C.-C. Lee, S.-M. Huang, H. Zheng, J. Ma, D. S. Sanchez, B. Wang, A. Bansil, F. Chou, P. P. Shibayev, H. Lin, S. Jia, and M. Z. Hasan, *Science* **249**, 613 (2015).
 - [19] C. Kane and T. C. Lubensky, *Nature Phys.* **10**, 39 (2014).
 - [20] T. C. Lubensky, C. L. Kane, X. Mao, A. Souslov, and K. Sun, *Rep. Prog. Phys.* **78**, 073901 (2015).
 - [21] J. Paulose, B. G. G. Chen, and V. Vitelli, *Nature Physics* **11**, 153 (2015).
 - [22] J. Paulose, A. S. Meeussen, and V. Vitelli, *Proc. Natl. Acad. Sci. USA* **112**, 7639 (2015).
 - [23] The term isostatic is often used to describe lattices with $N_B = dN$. Isostatic lattices are, however, strictly speaking Maxwell lattices with additional constraints. See Sec. 2.2.
 - [24] K. Sun, A. Souslov, X. Mao, and T. C. Lubensky, *PNAS* **109**, 12369 (2012).
 - [25] D. Z. Rocklin, B. G.-g. Chen, M. Falk, V. Vitelli, and T. Lubensky, *Phys. Rev. Lett.* **116**, 135503 (2016).
 - [26] H. C. Po, Y. Bahri, and A. Vishwanath, (2014), arXiv:1410.1320.
 - [27] O. Stenull, C. L. Kane, and T. C. Lubensky, arXiv:1606.00301 (2016).
 - [28] L. Lu, L. Fu, J. D. Joannopoulos, and M. Soljacic, *Nature Photonics* **7**, 294 (2013).
 - [29] A. B. Khanikaev, R. Fleury, S. H. Mousavi, and A. Al, *Nature Communications* **6** (2015).
 - [30] L. M. Nash, D. Kleckner, V. Vitelli, A. M. Turner, and W. T. M. Irvine, Arxiv:1504.03362 (2015), arXiv:1504.03362v1.
 - [31] Y.-T. Wang, P.-G. Luan, and S. Zhang, *New J. Phys.* **17**, 073031 (2015).
 - [32] P. Wang, L. Lu, and K. Bertoldi, *Phys. Rev. Lett.* **115**, 104302 (2015), 1079-7114.
 - [33] R. Suesstrunk and S. D. Huber, *Science* **349**, 47 (2015).
 - [34] Z. Yang, F. Gao, X. Shi, X. Lin, Z. Gao, Y. Chong, and B. Zhang, *Phys. Rev. Lett.* **114**, 114301 (2015).

- [35] V. Peano, C. Brendel, M. Schmidt, and F. Marquardt, Phys. Rev. X **5**, 031011 (2015).
- [36] M. Xiao, G. Ma, Z. Yang, P. Sheng, Z. Q. Zhang, and C. T. Chan, Nature Physics **11**, 240 (2015).
- [37] S. H. Mousavi, A. B. Khanikaev, and Z. Wang, Nature Communications **6**, 8682 (2015), 2041-1723.
- [38] T. Kariyado and Y. Hatsugai, arXiv:1505.06679 (2015).
- [39] M. Wyart, S. R. Nagel, and T. A. Witten, Europhys. Lett. **72**, 486 (2005).
- [40] M. Wyart, Ann. Phys. Fr **30**, 1 (2005).
- [41] D. M. Sussman, C. P. Goodrich, A. J. Liu, and S. R. Nagel, Soft Matter **11**, 2745 (2015).
- [42] C. S. O'Hern, L. E. Silbert, A. J. Liu, and S. R. Nagel, Phys. Rev. E **68**, 011306 (2003).
- [43] O. Stenull and T. C. Lubensky, Phys. Rev. Lett. **113**, 158301 (2014).
- [44] C. F. Moukarzel and G. G. Naumis, Phys. Rev. Lett. **115**, 209801 (2015).
- [45] O. Stenull and T. C. Lubensky, Phys. Rev. Lett. **115**, 209802 (2015).
- [46] S. S. Schoenholz, C. P. Goodrich, O. Kogan, A. J. Liu, and S. R. Nagel, Soft Matter **9**, 11000 (2013).
- [47] E. Bitzec, P. Koshkinen, F. Gähler, M. Moseler, and P. Gumbsch, Phys. Rev. Lett. **97**, 170201 (2006).
- [48] S. Alexander, Physics Reports **296**, 65 (1998).
- [49] M. Wyart, L. E. Silbert, S. R. Nagel, and T. A. Witten, Phys. Rev. E **72**, 051306 (2005).
- [50] N. D. de Bruijn, Proc. K. Ned. Acad. Wet. Ser. A **43**, 39 (1981).
- [51] R. Penrose, Bull. Inst. Math Appl. **10**, 266 (1974).
- [52] C. R. Calladine, Int. J. Solids Struct. **14**, 161 (1978).
- [53] A. Carpinteri, *Structural Mechanics - A Unified Approach* (Taylor and Francis, Abington, Oxon, 1997) see pages 139 and 147.
- [54] R. Connelly, P. W. Fowler, S. D. Guest, B. Schulze, and W. J. Whiteley, International Journal of Solids and Structures **46**, 762 (2009).
- [55] S. D. Guest and J. W. Hutchinson, J. Mech. Phys. Solids **51**, 383 (2003).
- [56] C. P. Goodrich, S. Dagois-Bohy, B. P. Tighe, M. van Hecke, A. J. Liu, and S. R. Nagel, Physical Review E **90** (2014), 10.1103/PhysRevE.90.022138.
- [57] M. Wyart, L. E. Silbert, S. R. Nagel, and T. A. Witten, Phys. Rev. E **72**, 051306 (2005).
- [58] E. DiGiuli, A. Laversanne-Finot, G. Düring, E. Lerner, and M. Wyart, Soft Matter **10**, 5628 (2014).
- [59] E. Yan, L. DiGiuli and M. Wyart, arXiv:1601.02141 (2016).
- [60] E. Lerner, G. Düring, and M. Wyart, Soft Matter **9**, 8252 (2013).
- [61] D. M. Sussman, C. P. Goodrich, and A. J. Liu, Soft Matter **12**, 3982 (2016).
- [62] B. G. Chen, <https://bitbucket.org/bryangingecheen/rigiditypackage>.